Cooling mechanical resonators to the quantum ground state from room temperature

Yong-Chun Liu,[1,2] Rui-Shan Liu,[1] Chun-Hua Dong,[3] Yan Li,[1,2] Qihuang Gong,[1,2] and Yun-Feng Xiao[1,2,*]

[1]*State Key Laboratory for Mesoscopic Physics and School of Physics, Peking University, Beijing 100871, People's Republic of China*

[2]*Collaborative Innovation Center of Quantum Matter, Beijing 100871, People's Republic of China*

[3]*Key Laboratory of Quantum Information, University of Science and Technology of China, Hefei 230026, People's Republic of China*

(Received 3 March 2014; published 15 January 2015)

Ground-state cooling of mesoscopic mechanical resonators is a fundamental requirement for testing of quantum theory and for implementation of quantum information. We analyze the cavity optomechanical cooling limits in the intermediate coupling regime, where the light-enhanced optomechanical coupling strength is comparable with the cavity decay rate. It is found that in this regime the cooling breaks through the limits in both the strong-coupling and the weak-coupling regimes. The lowest cooling limit is derived analytically under the optimal conditions of cavity decay rate and coupling strength. In essence, cooling to the quantum ground state requires $Q_{\rm m} > 2.4n_{\rm th}$, with $Q_{\rm m}$ being the mechanical quality factor and $n_{\rm th}$ being the thermal phonon number. Remarkably, ground-state cooling is achievable starting from room temperature, when the mechanical Q-frequency product $Q_{\rm m}\nu_{\rm m} > 1.5 \times 10^{13}$ Hz and both the cavity decay rate and the coupling strength exceed the thermal decoherence rate. Our study provides a general framework for optimizing the backaction cooling of mesoscopic mechanical resonators.

DOI: 10.1103/PhysRevA.91.013824 PACS number(s): 42.50.Wk, 07.10.Cm, 42.50.Lc

Cavity optomechanics [1–5] provides an important platform for manipulation of mesoscopic mechanical resonators in the quantum regime. A prominent example is motional ground-state cooling, which reduces the thermal noise of the mechanical resonator all the way to the quantum ground state [6,7]. This is offered as the first crucial step for most applications such as the exploration of quantum-classical boundary [8–10] and quantum information processing [11–13]. Although some mechanically mediated quantum phenomena can be observed under a modest number of thermal phonons [14–24], they can benefit from additional cooling. Recently cooling of mechanical resonators has been demonstrated using various approaches including pure cryogenic cooling [25], feedback cooling [26–30] and cavity-assisted backaction cooling [6,7,31–39], along with many theoretical and experimental efforts on novel cooling schemes, such as cooling with dissipative coupling [40–44], quadratic coupling [45], single-photon strong coupling [46], hybrid systems [47,48], laser pulse modulations [49–53], and dissipation modulations [54]. It is theoretically shown that ground-state cooling is possible in the resolved sideband regime [55–57], where the mechanical resonance frequency is greater than the decay rate of the optical cavity, indicating the resolved mechanical sideband from the cavity mode spectrum. These analyses are in the weak-coupling regime, where the light-enhanced optomechanical coupling strength G is weak compared with the cavity decay rate κ, and thus the coupling is regarded as a perturbation to the optical field. Within this regime a larger coupling strength is better since the net cooling rate (optical damping rate) scales as $\Gamma_{\rm wk} = 4G^2/\kappa$. On the other hand, when $G \gg \kappa$, the system is in the strong-coupling regime [54,58–63], where normal-mode splitting occurs and the phonon occupancy exhibits Rabi-like oscillation with reversible energy exchange between optical and mechanical modes. Then the cooling rate saturates with the maximum value of $\Gamma_{\rm str} = \kappa$, and thus a larger cavity decay rate κ is better. However, in this case, a large κ in turn takes the system away from the strong-coupling regime. As a result, the optimal cooling is expected for the intermediate-coupling regime, where the coupling strength G is comparable with the cavity decay rate κ.

In the weak-coupling regime, the perturbative approach [55,56] has been widely adopted. In the intermediate- and strong-coupling regimes, however, the perturbative approach fails since the optomechanical coupling can no longer be considered as a perturbation. One way to overcome this problem is to employ the covariance approach, where all the mean values of the second-order moments are computed with the linearized optomechanical interaction [54,59]. In this article, we use this nonperturbative approach to analyze the optimal cooling limits in the full parameter range and derive the optimal parameters, including laser detuning, cavity decay rate, and optomechanical coupling strength. We then find that the optimal cooling is reached with $G \sim 0.6\kappa$, which is in the intermediate-coupling regime. Finally we show the unique advantage of cooling in this regime, where room-temperature ground-state cooling is achievable for the mechanical Q-frequency product $Q_{\rm m}\nu_{\rm m} > 1.5 \times 10^{13}$, which is within reach for current experimental conditions [64,65].

We consider the general model of an optomechanical system, as shown in the inset of Fig. 1. A mechanical mode interacts with an optical resonance mode which is driven by a coherent laser. The system Hamiltonian reads $H = \omega_{\rm c}a^\dagger a + \omega_{\rm m}b^\dagger b + ga^\dagger a(b + b^\dagger) + (\Omega e^{-i\omega t}a^\dagger + \Omega^* e^{i\omega t}a)$. Here $\omega_{\rm c}$ ($\omega_{\rm m}$) is the angular resonance frequency of the optical mode a (mechanical mode b); the third term describes the optomechanical interaction [66], with g being the single-photon coupling rate; the last term describes the driving of the input laser with driving strength Ω and frequency ω. The coherent driving shifts the optical states and thereby shifts the mechanical states via the optical force. Thus the operators are rewritten as $a \to \alpha + a_1$ and $b \to \beta + b_1$, where α (β) represents the steady-state value of the optical (mechanical) mode and a_1 (b_1) stands for the corresponding

*yfxiao@pku.edu.cn; www.phy.pku.edu.cn/~yfxiao/index.html

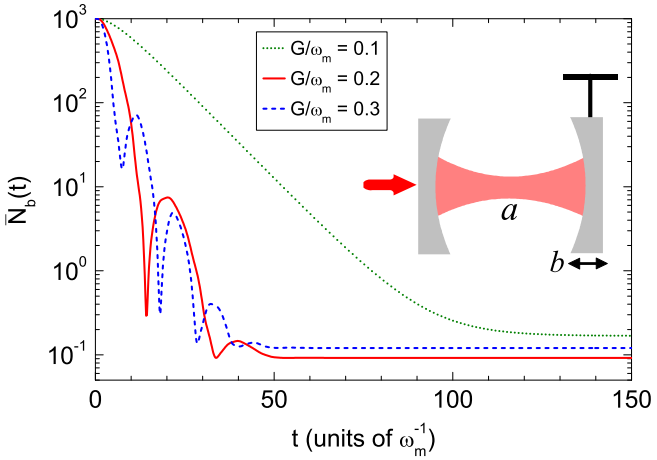

FIG. 1. (Color online) Time evolution of the mean phonon number $\bar{N}_b(t)$ for $G/\omega_{\rm m} = 0.1$ (green dotted curve), 0.2 (red solid curve), and 0.3 (blue dashed curve). Other parameters are $\Delta' = -\omega_{\rm m}$, $\kappa/\omega_{\rm m} = 0.5$, $\gamma/\omega_{\rm m} = 10^{-5}$, and $n_{\rm th} = 10^3$. Inset: Sketch of the optomechanical system.

fluctuation operator. For the strong intracavity field $|\alpha| \gg 1$, the Hamiltonian is approximated as a quadratic type given by $H_L = -\Delta' a_1^\dagger a_1 + \omega_{\rm m} b_1^\dagger b_1 + G(a_1^\dagger + a_1)(b_1 + b_1^\dagger)$, where $G = |\alpha| g$ describes the light-enhanced optomechanical-coupling strength and $\Delta' = \omega - \omega_{\rm c} + 2G^2/\omega_{\rm m}$ denotes the optomechanical-coupling modified detuning. In the above derivation we have absorbed the phase factor of α into the operator a.

The system evolution is governed by the master equation described by $\dot{\rho} = i[\rho, H_L] + \kappa \mathcal{D}[a_1]\rho + \gamma(n_{\rm th}+1)\mathcal{D}[b_1]\rho + \gamma n_{\rm th}\mathcal{D}[b_1^\dagger]\rho$. Here ρ is the density operator, $\mathcal{D}[\hat{o}]\rho = \hat{o}\rho\hat{o}^\dagger - (\hat{o}^\dagger\hat{o}\rho + \rho\hat{o}^\dagger\hat{o})/2$ ($\hat{o} = a_1, b_1, b_1^\dagger$) denotes the Lindblad dissipators, κ (γ) represents the dissipation rate of the optical cavity (mechanical) mode, and $n_{\rm th} = 1/(e^{\hbar\omega_{\rm m}/k_{\rm B}T} - 1)$ corresponds to the bath thermal phonon number at the environmental temperature T. Using the master equation, the mean phonon number $\bar{N}_b = \langle b_1^\dagger b_1\rangle = {\rm Tr}(\rho b_1^\dagger b_1)$ can be determined by a linear system of ordinary differential equations involving the mean values of all the second-order moments [54,59,67], i.e., $\partial_t\langle\hat{o}_i\hat{o}_j\rangle = {\rm Tr}(\dot{\rho}\hat{o}_i\hat{o}_j) = \sum_{k,l}\eta_{k,l}\langle\hat{o}_k\hat{o}_l\rangle$, where $\hat{o}_i$, $\hat{o}_j$, $\hat{o}_k$, and $\hat{o}_l$ are one of the operators a_1, b_1, $a_1^\dagger$, and $b_1^\dagger$. Initially, the mean phonon number is equal to the bath thermal phonon number, i.e., $\bar{N}_b(t=0) = n_{\rm th}$, and the mean values of other second-order moments are zero.

In Fig. 1, we plot the exact numerical results of the typical time evolution of the mean phonon number $\bar{N}_b(t)$ for various coupling strengths $G/\omega_{\rm m} = 0.1$, 0.2, and 0.3 with the given cavity decay rate $\kappa/\omega_{\rm m} = 0.5$. It can be found that, for $G = 0.2\kappa$, the mean phonon number decays monotonically, corresponding to the weak-coupling regime. As the coupling strength increases to $G = 0.4\kappa$, nonmonotonicity appears, which reveals that the system reaches the intermediate-coupling regime, with a lower steady-state cooling limit. For stronger coupling $G = 0.6\kappa$, the oscillations become more notable. However, the cooling limit is higher than that for $G = 0.4\kappa$, which is a result of the stronger quantum backaction.

To shed light on the lower cooling limit in the intermediate-coupling regime, we calculate the steady-state cooling limit in the full parameter range. By applying the Routh-Hurwitz criterion [68], it is found that the system reaches a steady state with the stability condition given by

$$\Delta' < 0, \tag{1a}$$

$$G^2 < \frac{(4\Delta'^2 + \kappa^2)\omega_{\rm m}}{16|\Delta'|}. \tag{1b}$$

Here Eq. (1a) implies the red detuning laser input, and Eq. (1b) shows that the coupling strength cannot be too strong. Under this condition, when the system reaches the steady state, the derivatives $\partial_t\langle\hat{o}_i\hat{o}_j\rangle$ all become zero, and thus the exact solutions for the steady-state cooling limits can be obtained by solving the algebraic equations ${\rm Tr}(\dot{\rho}\hat{o}_i\hat{o}_j) = 0$. The cooling limits can concisely be written as $n_{\rm s} = An_{\rm th} + B$, where A and B are expressions determined by the parameters Δ', $\omega_{\rm m}$, G, κ, and γ. To provide more physical insights, we divide the steady-state cooling limits into two parts:

$$n_{\rm s} = n_{\rm s}^{(1)} + n_{\rm s}^{(0)}. \tag{2}$$

Here $n_{\rm s}^{(1)} = An_{\rm th}$ describes the classical cooling limit, which originates from the mechanical dissipation and is proportional to the environmental thermal phonon number $n_{\rm th}$; $n_{\rm s}^{(0)} = B$ denotes the quantum cooling limit which originates from the quantum backaction and does not depend on $n_{\rm th}$.

In the unresolved sideband regime ($\kappa \gg \omega_{\rm m}$) where the mechanical sideband cannot be resolved from the cavity mode spectrum, the optimal quantum cooling limit is obtained at the detuning $\Delta' = -\kappa/2$ with $n_{\rm s}^{(0)} \simeq \kappa/(4\omega_{\rm m}) \gg 1$, which prevents ground-state cooling [55,56]. Thus, in the following we focus on the resolved sideband regime ($\omega_{\rm m} \gg \kappa$). In this case the optimal detunings for both the classical and the quantum cooling limits are near $\Delta' = -\omega_{\rm m}$, where the rotating-wave interaction characterized by the term $G(a_1^\dagger b_1 + a_1 b_1^\dagger)$ is on resonant, leading to the maximum energy transfer from the mechanical mode to the anti-Stokes sideband. Meanwhile, the counterrotating-wave interaction $G(a_1^\dagger b_1^\dagger + a_1 b_1)$ is off resonant, which has a minor contribution to the heating process. Under the conditions $\omega_{\rm m} \gg (\kappa, G) \gg \gamma$ and $\Delta' = -\omega_{\rm m}$, we obtain approximate analytical expressions of the cooling limits as

$$n_{\rm s}^{(1)}\big|_{\Delta'=-\omega_{\rm m}} \simeq \frac{4G^2+\kappa^2}{4G^2\kappa}\gamma n_{\rm th}, \tag{3a}$$

$$n_{\rm s}^{(0)}\big|_{\Delta'=-\omega_{\rm m}} \simeq \frac{\kappa^2+8G^2}{16\left(\omega_{\rm m}^2 - 4G^2\right)}. \tag{3b}$$

These limits are valid in the weak-, intermediate-, and strong-coupling regimes. In particular, in the weak-coupling regime ($\kappa \gg G$), the cooling limits reduce to $n_{\rm s}^{(1)} \simeq n_{\rm th}\gamma\kappa/(4G^2)$ and $n_{\rm s}^{(0)} \simeq \kappa^2/(16\omega_{\rm m}^2)$, which agree with the perturbation approaches [55,56]. For the strong-coupling regime ($G \gg \kappa$), the cooling limits are simplified as $n_{\rm s}^{(1)} \simeq n_{\rm th}\gamma/\kappa$ and $n_{\rm s}^{(0)} \simeq G^2/[2(\omega_{\rm m}^2 - 4G^2)]$.

In Fig. 2 we plot the exact numerical results of the cooling limits $n_{\rm s}^{(1)}$, $n_{\rm s}^{(0)}$, and $n_{\rm s}$ as functions of κ and G for $\Delta' = -\omega_{\rm m}$,

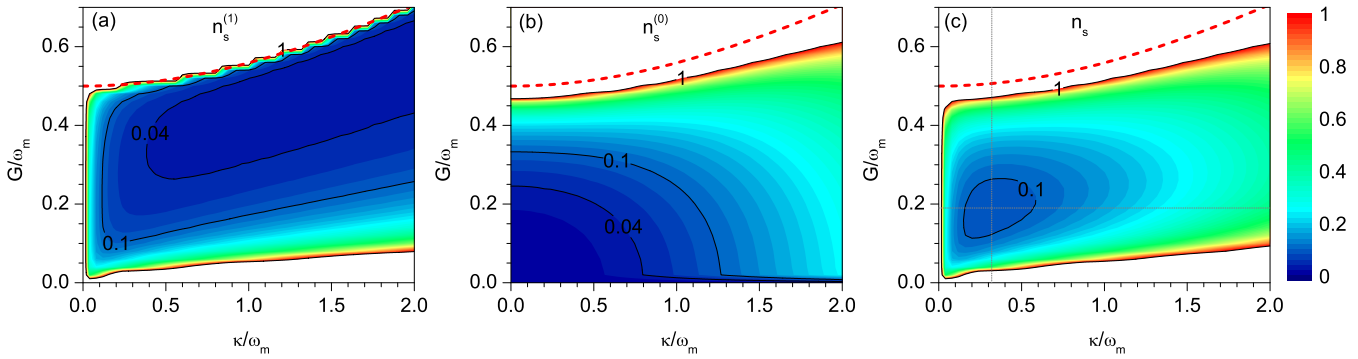

FIG. 2. (Color online) (a) Steady-state classical cooling limit $n_s^{(1)}$, (b) quantum cooling limit $n_s^{(0)}$, and (c) total cooling limit n_s as functions of the cavity decay rate κ and the coupling strength G. The red dashed curves correspond to the boundary of the stability condition given by Eq. (1b). In panel (c), the vertical and horizontal lines denote the optimal κ and G given by Eqs. (5a) and (5b). Other parameters are $\Delta' = -\omega_m$, $\gamma/\omega_m = 10^{-5}$, and $n_{th} = 10^3$.

$\gamma/\omega_m = 10^{-5}$, and $n_{th} = 10^3$. Near the boundary of the stable regions, the cooling limits rapidly increase. In the following we analyze the regions far away from the stability boundary. For the classical cooling limit $n_s^{(1)}$, a larger G (not large enough to reach the stability boundary) and a larger κ lead to a lower cooling limit, as shown in Fig. 2(a). Note that the classical cooling limit can be expressed as $n_s^{(1)} = n_{th}\gamma/\Gamma$, where Γ is the optical damping rate (net cooling rate) given by

$$\frac{1}{\Gamma} = \frac{1}{\Gamma_{wk}} + \frac{1}{\Gamma_{str}}, \tag{4a}$$

$$\Gamma_{wk} = \frac{4G^2}{\kappa}, \quad \Gamma_{str} = \kappa. \tag{4b}$$

Here Γ_{wk} and Γ_{str} represent the optical damping rate in the weak- and strong-coupling regimes, respectively. Therefore, for the weak-coupling case, to obtain a high cooling rate, one expects a large G^2/κ; while in the strong-coupling regime, a large κ leads to a high cooling rate.

On the other hand, a large G and a large κ result in a higher quantum cooling limit $n_s^{(0)}$ due to the stronger quantum backaction, as plotted in Fig. 2(b). These trade-offs result in optimal κ and G for the total cooling limit n_s, which can be approximately derived as

$$\kappa_{opt} \simeq 1.5\omega_m \left(\frac{n_{th}}{Q_m}\right)^{\frac{1}{3}}, \tag{5a}$$

$$G_{opt} \simeq 0.9\omega_m \left(\frac{n_{th}}{Q_m}\right)^{\frac{1}{3}}, \tag{5b}$$

where $Q_m = \omega_m/\gamma$ denotes the mechanical quality factor. It shows that $G_{opt} \sim 0.6\kappa_{opt}$, indicating the intermediate coupling. The gray dotted vertical and horizontal lines in Fig. 2(c) denote $\kappa = \kappa_{opt}$ and $G = G_{opt}$, which agree well with the numerical results.

In Fig. 3 we further plot $n_s^{(1)}$, $n_s^{(0)}$, and n_s for optimized G and κ, along the horizontal and vertical lines in Fig. 2(c), respectively. It shows that the classical cooling limit dominates for small κ and G, while the quantum cooling limit becomes important as κ and G increase, which are precisely described by Eqs. (3a) and (3b).

With the optimal parameters given in Eqs. (5a) and (5b), the optimal cooling limit reads

$$n_{opt} \simeq 1.8\left(\frac{n_{th}}{Q_m}\right)^{\frac{2}{3}}. \tag{6}$$

In Fig. 3(c) we plot n_{opt} as a function of the environmental temperature T for various Q-frequency products. This shows that a high Q-frequency product allows for achieving a low

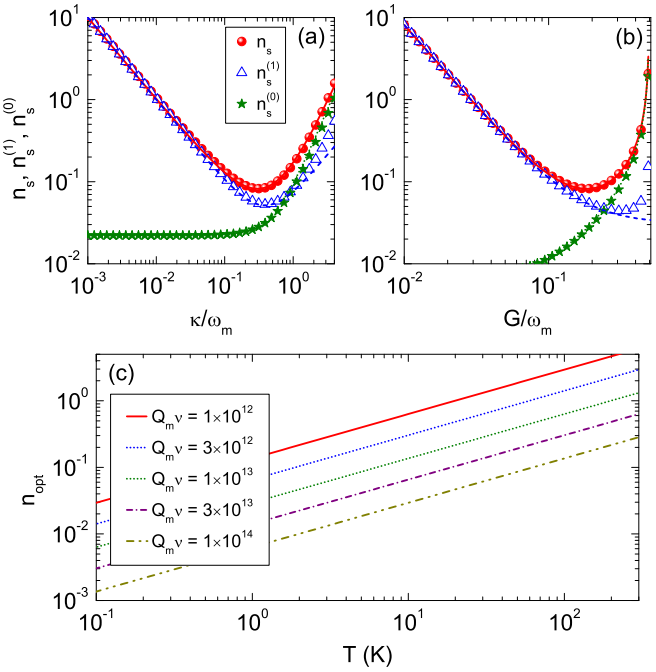

FIG. 3. (Color online) Cooling limits n_s (red circles and red solid curves), $n_s^{(1)}$ (blue triangles and blue dashed curves), and $n_s^{(0)}$ (green stars and green dotted curves) as functions of κ for $G = G_{opt}$ (a) and as functions of G for $\kappa = \kappa_{opt}$ (b). The circles, triangles, and stars are the numerical results, and the curves are the analytical results given by Eqs. (3a) and (3b). Other parameters are $\Delta' = -\omega_m$, $\gamma/\omega_m = 10^{-5}$, and $n_{th} = 10^3$. (c) n_{opt} as a function of the environmental temperature T for $Q_m\nu = 10^{12}$ (red solid curve), 3×10^{12} (blue dashed curve), 10^{13} (green dotted curve), 3×10^{13} (purple dash-dotted curve), and 10^{14} (orange dash-dot-dotted curve).

phonon number at a high-temperature region. For ground-state cooling (or ground-state occupancy probability $P > 50\%$), this requires

$$Q_{\rm m} > 2.4 n_{\rm th}. \tag{7}$$

For typical mechanical resonators, $\hbar\omega_{\rm m} \ll k_{\rm B}T$, and the thermal phonon number is approximated as $n_{\rm th} \simeq k_{\rm B}T/(\hbar\omega_{\rm m})$. Therefore, the condition (7) is equivalent to $Q_{\rm m}\omega_{\rm m} > 2.4 k_{\rm B}T/\hbar$, which provides a quantitative description compared with the qualitative analyses [56,69,70]. Starting from room temperature ($T = 300\,{\rm K}$), the requirement for ground-state cooling is expressed by the Q-frequency product

$$Q_{\rm m}\nu_{\rm m} > 1.5 \times 10^{13}\ {\rm Hz}, \tag{8}$$

where $\nu_{\rm m} = \omega_{\rm m}/2\pi$ is the mechanical resonance frequency.

In real experiments, there are restrictions on the cavity decay rate κ and the coupling strength G. For example, many optical cavities have lower bounds for κ due to the limitation of fabrication and material absorption. The coupling strength G is related to the intracavity optical field, while a strong light field usually leads to material absorption and heating. Therefore, it is important to take these constraints into consideration. In the following we provide the parameter ranges for κ and G where ground-state cooling can be reached.

First we consider the requirement for the cavity decay rate κ. The optimal coupling strength G for a given κ is obtained as

$$G_{\rm opt}(\kappa) \simeq \left(\frac{\omega_{\rm m}^2 \kappa \gamma n_{\rm th}}{2}\right)^{\frac{1}{4}}. \tag{9}$$

Under this condition, ground-state cooling requires

$$\gamma n_{\rm th} < \kappa < 4\omega_{\rm m}. \tag{10}$$

The left inequality reveals that the cavity decay rate should exceed the thermal decoherence rate $\Gamma_{\rm th} = \gamma n_{\rm th}$ to suppress the environmental heating. The requirement can be re-expressed as $Q_{\rm m}\kappa > k_{\rm B}T/\hbar$. At room temperature, it yields

$$Q_{\rm m}\kappa > 6.2 \times 10^{12}\ {\rm Hz}. \tag{11}$$

The right inequality in Eq. (10) shows that the resolved sideband condition should be satisfied to reduce the quantum backaction heating. In Fig. 4(a) the exact numerical results for the ground-state region are plotted, with the region boundary being well described by Eq. (10). As an example, we plot the cooling limit $n_{\rm s}$ as a function of κ for $\gamma/\omega_{\rm m} = 10^{-5}$ and $n_{\rm th} = 10^3$ in Fig. 4(b). In this case $n_{\rm s} < 1$ requires $0.01 < \kappa/\omega_{\rm m} < 4$.

Then we analyze the requirement for the coupling strength G. We determine the optimal cavity decay rate κ for a given G as

$$\kappa_{\rm opt}(G) \simeq 2G. \tag{12}$$

Then the requirement for ground-state cooling is given by

$$\gamma n_{\rm th} < G < 0.5\omega_{\rm m}. \tag{13}$$

Clearly, the coupling strength should also exceed the thermal decoherence rate to suppress the environmental heating, and room-temperature ground-state cooling requires

$$Q_{\rm m}G > 6.2 \times 10^{12}\ {\rm Hz}. \tag{14}$$

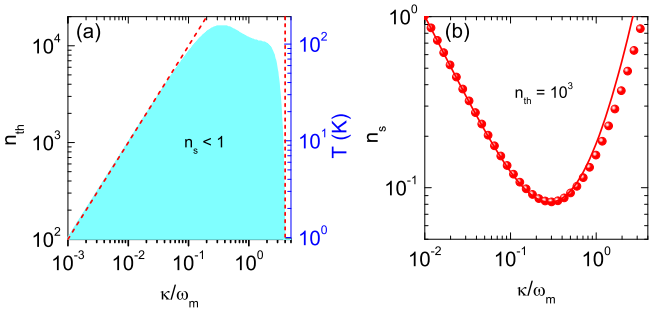

FIG. 4. (Color online) (a) Contour plot of the ground-state region ($n_{\rm s} < 1$) as functions of κ and $n_{\rm th}$. The shaded region corresponds to $n_{\rm s} < 1$. The red dashed lines denote $\kappa = \gamma n_{\rm th}$ (left) and $\kappa = 4\omega_{\rm m}$ (right), respectively. (b) Cooling limit $n_{\rm s}$ as a function of κ for $n_{\rm th} = 10^3$. The red circles are the numerical results and the red solid curve corresponds to the analytical results given by Eqs. (3a) and (3b). Other parameters are $\Delta' = -\omega_{\rm m}$, $\gamma/\omega_{\rm m} = 10^{-5}$, and $G = G_{\rm opt}(\kappa)$ [given by Eq. (9)].

In Eq. (13) the upper restriction $G < 0.5\omega_{\rm m}$ is limited by the stability condition given by Eq. (1b). In Fig. 5(a) the exact numerical results for the ground-state region are plotted, with the region boundary being well described by Eq. (13). The cooling limit as a function of G for $n_{\rm th} = 10^3$ is shown in Fig. 5(b).

In summary, we have examined the backaction cooling of mesoscopic mechanical resonators in the intermediate-coupling regime. We develop a general framework to describe the steady-state backaction cooling limits in the full parameter range. We have analytically derived the optimal cooling limits and the optimal parameters including the cavity decay rate and the optomechanical coupling strength. In the resolved sideband regime, under the optimal detuning $\Delta' = -\omega_{\rm m}$, the optimal cavity decay rate and the optimal coupling strength are derived as $\kappa_{\rm opt}/\omega_{\rm m} \simeq 1.5(n_{\rm th}/Q_{\rm m})^{1/3} \simeq (2.1 \times 10^{13}/Q_{\rm m}\nu_{\rm m})^{1/3}$ and $G_{\rm opt}/\omega_{\rm m} \simeq 0.9(n_{\rm th}/Q_{\rm m})^{1/3}$, with the lowest cooling limit being $n_{\rm opt} \simeq 1.8(n_{\rm th}/Q_{\rm m})^{2/3} \simeq (1.5 \times 10^{13}/Q_{\rm m}\nu_{\rm m})^{2/3}$. At the optimal point, the requirement for ground-state cooling is $Q_{\rm m} > 2.4 n_{\rm th}$. Starting from room temperature, ground-state cooling is achievable for the mechanical Q-frequency product $Q_{\rm m}\nu_{\rm m} > 1.5 \times 10^{13}$ Hz. For practical optomechanical systems, the allowed parameter regions for ground-state cooling are $\gamma n_{\rm th} < \kappa < 4\omega_{\rm m}$ and $\gamma n_{\rm th} < G < 0.5\omega_{\rm m}$. This provides a guideline for achieving the lowest cooling limit

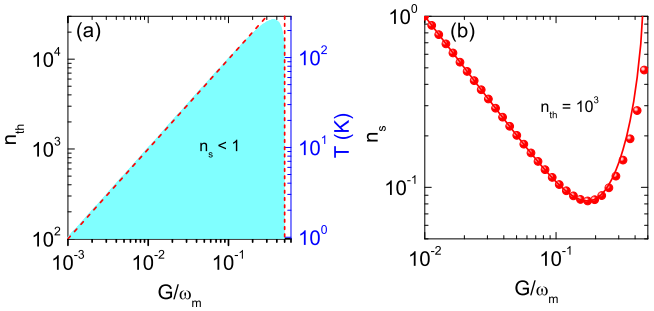

FIG. 5. (Color online) Same as Fig. 4 except that the horizontal axes are G and the value of the cavity decay rate is $\kappa = \kappa_{\rm opt}(G)$ [given by Eq. (12)]. In panel (a), the red dashed lines denote $G = \gamma n_{\rm th}$ (left) and $G = 0.5\omega_{\rm m}$ (right), respectively.

towards room-temperature ground-state cooling of mechanical resonators. For recent experiments [65] with parameters $Q_m = 5 \times 10^7$, $\nu_m = 2$ MHz, and $Q_m \nu_m = 10^{14}$ Hz, under the optimal cavity decay rate $\kappa_{opt} \simeq 1.2$ MHz and the optimal coupling strength $G_{opt} \simeq 0.7$ MHz, the minimum phonon number of $n_{opt} \simeq 0.3$ can be reached.

This work is supported by the 973 Program (Grants No. 2013CB921904 and No. 2013CB328704), the NSFC (Grants No. 61435001, No. 11474011, No. 11222440, and No. 11121091), and RFDPH (Grant No. 20120001110068). R.S.L. was supported by the National Fund for Fostering Talents of Basic Science (Grants No. J1030310 and No. J1103205).

[1] T. J. Kippenberg and K. J. Vahala, Science **321**, 1172 (2008).
[2] F. Marquardt and S. M. Girvin, Physics **2**, 40 (2009).
[3] P. Meystre, Ann. Phys. (Berlin) **525**, 215 (2013).
[4] M. Aspelmeyer, T. J. Kippenberg, and F. Marquardt, Rev. Mod. Phys. **86**, 1391 (2014).
[5] Y.-C. Liu, Y.-W. Hu, C. W. Wong, and Y.-F. Xiao, Chin. Phys. B **22**, 114213 (2013).
[6] J. D. Teufel, T. Donner, D. Li, J. W. Harlow, M. S. Allman, K. Cicak, A. J. Sirois, J. D. Whittaker, K. W. Lehnert, and R. W. Simmonds, Nature (London) **475**, 359 (2011).
[7] J. Chan, T. P. Mayer Alegre, A. H. Safavi-Naeini, J. T. Hill, A. Krause, S. Gröblacher, M. Aspelmeyer, and O. Painter, Nature (London) **478**, 89 (2011).
[8] O. Romero-Isart, A. C. Pflanzer, F. Blaser, R. Kaltenbaek, N. Kiesel, M. Aspelmeyer, and J. I. Cirac, Phys. Rev. Lett. **107**, 020405 (2011).
[9] B. Pepper, R. Ghobadi, E. Jeffrey, C. Simon, and D. Bouwmeester, Phys. Rev. Lett. **109**, 023601 (2012).
[10] Z.-q. Yin, T. Li, X. Zhang, and L. M. Duan, Phys. Rev. A **88**, 033614 (2013).
[11] S. Mancini, D. Vitali, and P. Tombesi, Phys. Rev. Lett. **90**, 137901 (2003).
[12] K. Stannigel, P. Rabl, A. S. Sørensen, P. Zoller, and M. D. Lukin, Phys. Rev. Lett. **105**, 220501 (2010).
[13] K. Stannigel, P. Komar, S. J. M. Habraken, S. D. Bennett, M. D. Lukin, P. Zoller, and P. Rabl, Phys. Rev. Lett. **109**, 013603 (2012).
[14] Y.-D. Wang and A. A. Clerk, Phys. Rev. Lett. **108**, 153603 (2012).
[15] L. Tian, Phys. Rev. Lett. **108**, 153604 (2012).
[16] S. Barzanjeh, M. Abdi, G. J. Milburn, P. Tombesi, and D. Vitali, Phys. Rev. Lett. **109**, 130503 (2012).
[17] Y. Liu, M. Davanco, V. Aksyuk, and K. Srinivasan, Phys. Rev. Lett. **110**, 223603 (2013).
[18] D. Vitali, S. Gigan, A. Ferreira, H. R. Bohm, P. Tombesi, A. Guerreiro, V. Vedral, A. Zeilinger, and M. Aspelmeyer, Phys. Rev. Lett. **98**, 030405 (2007).
[19] L. Tian, Phys. Rev. Lett. **110**, 233602 (2013).
[20] Y.-D. Wang and A. A. Clerk, Phys. Rev. Lett. **110**, 253601 (2013).
[21] C. Dong, V. Fiore, M. C. Kuzyk, and H. Wang, Science **338**, 1609 (2012).
[22] J. T. Hill, A. H. Safavi-Naeini, J. Chan, and O. Painter, Nat. Commun. **3**, 1196 (2012).
[23] H.-K. Li, X.-X. Ren, Y.-C. Liu, and Y.-F. Xiao, Phys. Rev. A **88**, 053850 (2013).
[24] M. C. Kuzyk, S. J. van Enk, and H. Wang, Phys. Rev. A **88**, 062341 (2013).
[25] A. D. O'Connell, M. Hofheinz, M. Ansmann, R. C. Bialczak, M. Lenander, E. Lucero, M. Neeley, D. Sank, H. Wang, M. Weides, J. Wenner, J. M. Martinis, and A. N. Cleland, Nature (London) **464**, 697 (2010).
[26] S. Mancini, D. Vitali, and P. Tombesi, Phys. Rev. Lett. **80**, 688 (1998).
[27] P.-F. Cohadon, A. Heidmann, and M. Pinard, Phys. Rev. Lett. **83**, 3174 (1999).
[28] D. Kleckner and D. Bouwmeester, Nature (London) **444**, 75 (2006).
[29] T. Corbitt, C. Wipf, T. Bodiya, D. Ottaway, D. Sigg, N. Smith, S. Whitcomb, and N. Mavalvala, Phys. Rev. Lett. **99**, 160801 (2007).
[30] M. Poggio, C. L. Degen, H. J. Mamin, and D. Rugar, Phys. Rev. Lett. **99**, 017201 (2007).
[31] S. Gigan, H. R. Böhm, M. Paternostro, F. Blaser, G. Langer, J. B. Hertzberg, K. C. Schwab, D. Bäuerle, M. Aspelmeyer, and A. Zeilinger, Nature (London) **444**, 67 (2006).
[32] O. Arcizet, P.-F. Cohadon, T. Briant, M. Pinard, and A. Heidmann, Nature (London) **444**, 71 (2006).
[33] A. Schliesser, P. Del'Haye, N. Nooshi, K. J. Vahala, and T. J. Kippenberg, Phys. Rev. Lett. **97**, 243905 (2006).
[34] A. Schliesser, R. Rivière, G. Anetsberger, O. Arcizet, and T. J. Kippenberg, Nat. Phys. **4**, 415 (2008).
[35] S. Gröblacher, J. B. Hertzberg, M. R. Vanner, G. D. Cole, S. Gigan, K. C. Schwab, and M. Aspelmeyer, Nat. Phys. **5**, 485 (2009).
[36] Y.-S. Park and H. Wang, Nat. Phys. **5**, 489 (2009).
[37] A. Schliesser, O. Arcizet, R. Rivère, G. Anetsberger, and T. J. Kippenberg, Nat. Phys. **5**, 509 (2009).
[38] T. Rocheleau, T. Ndukum, C. Macklin, J. B. Hertzberg, A. A. Clerk, and K. C. Schwab, Nature (London) **463**, 72 (2010).
[39] R. Riviere, S. Deleglise, S. Weis, E. Gavartin, O. Arcizet, A. Schliesser, and T. J. Kippenberg, Phys. Rev. A **83**, 063835 (2011).
[40] F. Elste, S. M. Girvin, and A. A. Clerk, Phys. Rev. Lett. **102**, 207209 (2009).
[41] M. Li, W. H. P. Pernice, and H. X. Tang, Phys. Rev. Lett. **103**, 223901 (2009).
[42] A. Xuereb, R. Schnabel, and K. Hammerer, Phys. Rev. Lett. **107**, 213604 (2011).
[43] T. Weiss and A. Nunnenkamp, Phys. Rev. A **88**, 023850 (2013).
[44] M.-Y. Yan, H.-K. Li, Y.-C. Liu, W.-L. Jin, and Y.-F. Xiao, Phys. Rev. A **88**, 023802 (2013).
[45] A. Nunnenkamp, K. Børkje, J. G. E. Harris, and S. M. Girvin, Phys. Rev. A **82**, 021806(R) (2010).
[46] A. Nunnenkamp, K. Børkje, and S. M. Girvin, Phys. Rev. A **85**, 051803(R) (2012).

[47] C. Genes, H. Ritsch, and D. Vitali, Phys. Rev. A **80**, 061803(R) (2009).
[48] B. Vogell, K. Stannigel, P. Zoller, K. Hammerer, M. T. Rakher, M. Korppi, A. Jöckel, and P. Treutlein, Phys. Rev. A **87**, 023816 (2013).
[49] M. R. Vanner, I. Pikovski, G. D. Cole, M. S. Kim, Č. Brukner, K. Hammerer, G. J. Milburn, and M. Aspelmeyer, Proc. Natl. Acad. Sci. USA **108**, 16182 (2011).
[50] Y. Li, L.-A. Wu, and Z. D. Wang, Phys. Rev. A **83**, 043804 (2011).
[51] J.-Q. Liao and C. K. Law, Phys. Rev. A **84**, 053838 (2011).
[52] X. Wang, S. Vinjanampathy, F. W. Strauch, and K. Jacobs, Phys. Rev. Lett. **107**, 177204 (2011).
[53] S. Machnes, J. Cerrillo, M. Aspelmeyer, W. Wieczorek, M. B. Plenio, and A. Retzker, Phys. Rev. Lett. **108**, 153601 (2012).
[54] Y.-C. Liu, Y.-F. Xiao, X. Luan, and C. W. Wong, Phys. Rev. Lett. **110**, 153606 (2013).
[55] I. Wilson-Rae, N. Nooshi, W. Zwerger, and T. J. Kippenberg, Phys. Rev. Lett. **99**, 093901 (2007).
[56] F. Marquardt, J. P. Chen, A. A. Clerk, and S. M. Girvin, Phys. Rev. Lett. **99**, 093902 (2007).
[57] C. Genes, D. Vitali, P. Tombesi, S. Gigan, and M. Aspelmeyer, Phys. Rev. A **77**, 033804 (2008).
[58] J. M. Dobrindt, I. Wilson-Rae, and T. J. Kippenberg, Phys. Rev. Lett. **101**, 263602 (2008).
[59] I. Wilson-Rae, N. Nooshi, J. Dobrindt, T. J. Kippenberg, and W. Zwerger, New J. Phys. **10**, 095007 (2008).
[60] S. Gröblacher, K. Hammerer, M. R. Vanner, and M. Aspelmeyer, Nature (London) **460**, 724 (2009).
[61] J. D. Teufel, D. Li, M. S. Allman, K. Cicak, A. J. Sirois, J. D. Whittaker, and R. W. Simmonds, Nature (London) **471**, 204 (2011).
[62] E. Verhagen, S. Deléglise, S. Weis, A. Schliesser, and T. J. Kippenberg, Nature (London) **482**, 63 (2012).
[63] T. A. Palomaki, J. W. Harlow, J. D. Teufel, R. W. Simmonds, and K. W. Lehnert, Nature (London) **495**, 210 (2013).
[64] D. J. Wilson, C. A. Regal, S. B. Papp, and H. J. Kimble, Phys. Rev. Lett. **103**, 207204 (2009).
[65] S. Chakram, Y. S. Patil, L. Chang, and M. Vengalattore, Phys. Rev. Lett. **112**, 127201 (2014).
[66] C. K. Law, Phys. Rev. A **51**, 2537 (1995).
[67] Y.-C. Liu, Y.-F. Shen, Q. Gong, and Y.-F. Xiao, Phys. Rev. A **89**, 053821 (2014).
[68] E. X. DeJesus and C. Kaufman, Phys. Rev. A **35**, 5288 (1987).
[69] Z.-q. Yin, Phys. Rev. A **80**, 033821 (2009).
[70] D. E. Chang, K.-K. Ni, O. Painter, and H. J. Kimble, New J. Phys. **14**, 045002 (2012).